Construction and Building Materials xxx (xxxx) xxx

Contents lists available at ScienceDirect

Construction and Building Materials

journal homepage: www.elsevier.com/locate/conbuildmat

A unified fractional breakage model for granular materials inspired by the crushing tests of dyed gypsum particles

Chao-Min Shen, Ji-Du Yu *, Si-Hong Liu *, Hang-Yu Mao

College of Water Conservancy and Hydropower Engineering, Hohai University, Nanjing 210098, China

HIGHLIGHTS

- A novel method using dyed gypsum particles to study particle breakage was proposed.
- Fractional particle breakage in different granular assemblies showed unified evolution path.
- A unified simple fractional particle breakage evolution model was established.
- The model performed well in predicting the PSD evolution of initially polydisperse particles.

ARTICLE INFO

Article history:
Received 20 June 2020
Received in revised form 25 August 2020
Accepted 16 October 2020
Available online xxxx

Keywords:
Granular materials
Particle breakage
Plastic work
Confined comminution

ABSTRACT

Particle breakage of granular materials is a phenomenon of great importance in engineering practices. This paper presents a unified particle breakage model for granular materials, which is able to capture the evolution of the particle size distribution (PSD) of each size fraction of particles. A novel experimental technique using dyed gypsum particles (DGPs) to track the fractional particle breakage was first adopted in the one-dimensional compression tests. A unique path of the fractional particle breakage, regardless of whether the particles were in a polydisperse medium or in other different granular assemblies, was then experimentally identified. This result has inspired the introduction of the definition of a fractional breakage index, based on which the breakage-plastic work relationship for overall granular assemblies was extended to describe the fractional particle breakage. The established fractional particle breakage model differs from most existing particle breakage models in that it is able to capture both the evolution of the fractional and the overall PSDs of granular materials, even when the initial PSD of the granular material surpassed partially the theoretical fractal PSD. These results set a vision to predict and understand the particle breakage of granular materials in industrial activities.

1. Introduction

Particle breakage of granular materials is an important phenomenon that has given rise to increasing concern due to both its scientific and engineering interest. In particular, particle breakage in civil engineering, such as driving piles in sands, settlement of high rockfill dams, and compaction of graded crushed rocks [1–4], has raised the question of how to quantify its influence on the mechanical response of granular soils. Extensive efforts, ranging from laboratory tests to physically-based analyses, e.g., micromechanical and thermodynamic analyses [5–9], have pointed out that the grain crushing of particles in granular media must be related to the change of the particle size distribution (PSD), so that the amount of particle breakage, as well as its relationship with the mechanical properties can be measured.

The evolution of the PSD can be measured by conducting conventional sieving tests on parallel specimens at different stages of loading [10–16]. As the conventional sieving tests can only obtain the collective particle breakage, a lot of detailed information during grain crushing cannot be observed. X-ray tomography, which was often used in granular physics to investigate the tomography of the contact fabric, has also been used to understand the mechanism of the particle breakage [17–19]. Other experimental techniques, such as high-speed camera method, are also proven to be effective in inspecting the particle breakage [20–22] . DEM simulations have been proven to be another powerful tool in capturing the micromechanical behavior during particle breakage. Different particle breakage simulation techniques in DEM, including agglomerate method [23–25] and particle splitting method[26–27] have been widely used to reveal more detailed information

* Corresponding authors.
E-mail addresses: chaomin.shen@hotmail.fr (C.-M. Shen), yujidu@hhu.edu.cn (J.-D. Yu), sihongliu@hhu.edu.cn (S.-H. Liu), hymao@hhu.edu.cn (H.-Y. Mao).

https://doi.org/10.1016/j.conbuildmat.2020.121366
0950-0618/

Nomenclature

a	material constant for a given granular soil, see equation (15)
B_r	Einav's relative breakage index
$B_r(d)$	fractional breakage index
d	particle size
d_0	reference particle size, see equation (19)
d_i	characteristic particle size of fraction i
d_m, d_M	minimum and maximum particle size
D	fractal dimension
m	Weibull modulus
$p_0(d)$	initial particle size distribution for the whole sample
$P_0(d)$, $P(d)$, $P_u(d)$	initial, current and ultimate cumulative mass distribution
$P_{f0}(d_i, d)$, $P_f(d_i, d)$, $P_{fu}(d_i, d)$	initial, current and ultimate mass percentage of particles smaller than d for the fractional particles with characteristic size d_i. same definitions for $P_{f0}(\Delta, d)$, $P_f(\Delta, d)$, $P_{fu}(\Delta, d)$
$P_s(\sigma, d)$	survival probability of particles with size d under stress σ
$V_0(d)$	Cumulative volume of particles with initial sizes small than d
V_0^t	initial total volume of a granular assembly
$\mathrm{d}W_p(d)$	plastic work input into the particles with initial sizes ranging from d to d + dd
$w_p(d)$	plastic work input per unit volume of particles of size d in a granular assembly
W_p^t	total plastic work input of a granular assembly
w_p^t	total plastic work input per unit volume of a granular assembly
X_i	mass percentage of fraction i
α	size-independent material parameter related to the plastic work input per unit increase of the fractional breakage index, see equation (24)
β	material parameter related to the initial particle size distribution, see equation (12)
ε_v^p	plastic volumetric strain
$\theta(d)$	probability density of the plastic work in a granular system
λ	material parameter reflecting the particle size effect, see equation (21)
σ_0	reference stress, see equation (16)
σ_v	vertical stress

(e.g., contact force distribution, fabric evolution, energy dissipation). Recently, more advanced numerical methods, such as FDEM [28–30] and *peri*-dynamics [31] have been used by a number of authors to reproduce more realistic particle breakage.

Various methods for quantifying the evolution of the PSDs of granular materials during grain crushing have been proposed. A group of practical approaches based on the concept of relative breakage, have been developed to define the degree to which the granular material is crushed during loading [10,32–34]. A key component in the concept of relative breakage is a predefined ultimate PSD that "guides" and eventually slows down the evolution of the PSD. In the pioneering work using this approach by Hardin [32], it was assumed that all particles in a granular medium will be crushed to the extent that no particles remain larger than 0.074 mm. This assumption, however, contradicts the fact that the PSDs of most granular materials undergoing substantial grain crushing tend to become self-similar, also known as fractal [16,35]. Einav [34] replaced Hardin's ultimate PSD with a fractal distribution and assumed that the evolution of the current PSD can be represented by linear interpolation of the initial and the ultimate PSDs with the aid of the defined relative breakage index. In spite of the simplicity and the thermodynamic insight provided, the relative breakage indexes were defined in a continuum mechanics context and thus omit the breakage of particles with different sizes.

Statistical approaches have also been widely used to relate the fractional particle breakage and the evolution of the PSD of the granular continuum. Extensive evidence shows that the crushing strength depends statistically on both the intrinsic properties of particles (e.g., particle minerology, particle shape and the particle size [36–39] and the coordination number [16,40], namely, the number of contacting particles in the granular assembly. McDowell and Bolton [41] modified the Weibull statistics by emphasizing the importance of the coordination number and found a fractal distribution of particles emerging from the compression of an aggregate of uniform grains. A more effective alternative is to use the Markov chain model to link the probability of particles within a given size range and the current PSD of the material. Similar methods, such as the population balance model and the combined linear packing and Markov chain model [42,43] were also proposed to model the fractional particle breakage. As the evolution of the current PSD or the coordination number in a polydisperse granular packing cannot be easily obtained, numerical simulations that discretize the loading path and the particle size has to be adopted in these models. As a result, although the probabilistic models are able to describe the fractional particle breakage, these models require incremental matrix computation to predict the evolution of the PSD, which lacks the simplicity compared to the relative breakage index defined in the continuum mechanics context. For this reason, most of the probabilistic models cannot be used in constitutive modelling of crushable granular materials, not to mention the numerical implementation in engineering practices.

The aim of this study is thus to establish a simple model for predicting the evolution of the fractional particle breakage of polydisperse granular materials. To this end, the 1D compression test results on artificially dyed granular materials are first presented to provide detailed and realistic fractional particle breakage observations. Afterwards, a unified model for predicting the particle breakage of granular materials is proposed. The performance of the fractional particle breakage model is validated by comparing with available experimental data.

2. Compression tests on dyed granular material

Prior to establishing the fractional breakage model, the following issue needs to be addressed: How to experimentally observe the evolution of the fractional PSDs during particle breakage? As it is difficult to track the fractional particle breakage in conventional crushing tests, the understanding of fractional breakage is very limited so far. In this section, we designed a novel technique which consists of using dyed gypsum particles (DGPs) in compression tests to address this issue. The idea of using the dying technique to track the particles in granular assemblies was inspired by Nakata et al. [44] who seeded a small group of surface-dyed silica sands into triaxial samples to test the survival probability. Herein the use of the artificial DGPs rather than the dyed natural granular particles is intended to ensure that the inside of the test particles was completely dyed so that we can clearly distinguish the color of the particles even after several generations of breakage.

2.1. Test procedure

2.1.1. Preparation of dyed gypsum particles (DGPs)

Gypsum ($CaSO_4$) is a widely used industrial and building material. To ensure that the strength of the produced DGPs is similar to that of typical granular materials, we used the α-hemihydrate gypsum powder (α-$CaSO_4{\cdot}1/2H_2O$), with a 2-hour flexural strength of 7 MPa, an initial setting time of 8 min, and a demolding time of 30 min. The optimal mixing ratio of the gypsum powder, water, and pigment was determined at 1: 0.34: 0.02. After a sufficient stirring process in the gypsum paste, the gypsum mold was put on the vibrating machine to discharge the inner bubbles in the paste until the paste solidifies. This procedure was to guarantee the high strength and the homogeneity of the produced particles. After demolding, the gypsum board was put in the curing room with a surrounding temperature of 20 ℃ for 24 h. Then, the gypsum board was mechanically crushed with varying amounts of inputting work to produce the DGPs with specific sizes. Five colors of gypsum boards were prepared, that is, blue, yellow, red, green, and grey, and they were crushed into particles with sizes of 2.0–3.1, 3.1–5.0, 5.0–7.9, 7.9–12.6, and 12.6–20.0 mm, respectively. The specific gravity of DGPs was measured to be 2.3. Fig. 1 displays the photos of the artificial DGPs. To avoid the maldistribution of size in one group of particles, an intermediate particle size $d_{imid} = \sqrt{d_{imin}d_{imax}}$ was added in each size interval, where d_{imin} and d_{imax} represent the minimum and maximum particle size of size group *i*. In this study, the mixing ratio of the two parts in each size group was set at 1:1, so that the corresponding median sizes (d_{50}) of the above batches of particles were 2.5, 4.0, 6.3, 10.0, and 15.9 mm, respectively. It is worth mentioning that DGPs with different sizes showed similar geometrics (four shape factors were measured, namely, convexity, sphericity, aspect ratio, and flatness, the average values of which changed from 0.946 to 0.961, 0.908 to 0.938, 0.710 to 0.720, and 0.499 to 0.511, respectively) [45–47], which indicated that the influence of particle morphology on the following tests can be neglected.

2.1.2. One-dimensional compression tests

A series of one-dimensional compression tests on the DGPs were conducted by varying the initial PSDs and the applied vertical stresses. The detailed information regarding the initial PSDs, initial void ratios and applied vertical stresses of the DGP samples were listed in Table 1. DGP samples of twelve different initial PSDs, including uniform gradings (U1-U5), polydisperse gradings (M2, M3 and M5-M7), and gap gradings (M1 and M4) were tested. The specimen of each grading weighed 600 g, with a diameter of 100 mm. All specimens were packed to the densest state. To observe the evolution of particle breakage, all gradings were compressed to four different vertical stress levels, i.e., 0.8 MPa, 1.6MP, 3.2 MPa, and 6.4 MPa, except for M1, M3 and M4, which were only compressed to the maximum vertical stress of 6.4 MPa. After the compression, the DGPs were sieved and then the particles were separated by color. Because particles within the same initial size range were of the same color, the technique of using DGPs provides a useful tool in knowing which original size range were the crushed particles from.

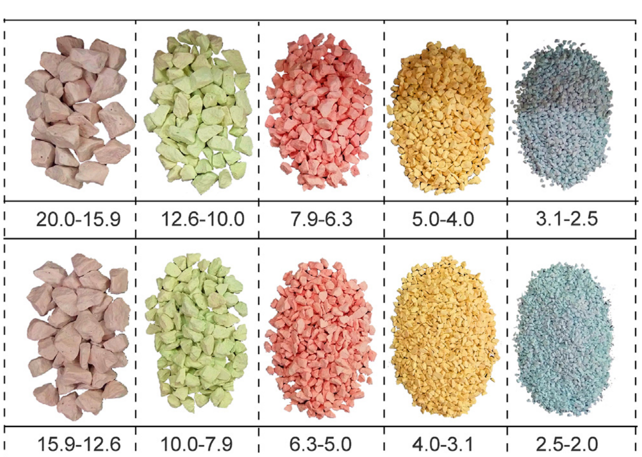

Fig. 1. Snapshots of dyed gypsum particles of different initial sizes.

2.2. Results and discussion

The one-dimensional compression curves of the DGP samples are plotted in Fig. 2. The curves are approximately linear under relatively high stresses on the semi-log plot, which were commonly observed in the compression tests of crushable granular materials [11,40]. The compression lines of the uniform DGP samples tend to converge at high stress levels, whereas the compression lines for non-uniform DGP samples are not unique at high stress levels. Comparing with uniform samples, the polydisperse samples with a wider size distribution are generally less compressible. The compression characteristics of the dyed gypsum material agree well with the experimental results of silica sand by Altuhafi and Coop [11] and the DEM results by Minh and Cheng [40]. This agreement indicates that the DGP is a typical brittle granular material and can be applied to explore the breakage behavior of granular materials.

Thanks to the color tracking method, we can obtain the PSDs of each size fraction of particles. Note that in this study we consider particles of a certain size range of the initial sample as one fraction. Fig. 3 plots the PSDs of the whole sample (PSD-W) and of each fraction (PSD-F) together. It is readily seen that the PSD-W equals the weighted sum of the PSD-Fs

$$P(d) = \sum_{i=1}^{N} X_i P_f(d_i,\ d) \tag{1}$$

where *i* denotes the serial number of fractions, ranging from 1 to *N*; d_i denotes the characteristic size of fraction *i*; $P(d)$ and $P_f(d_i,\ d)$ denote the percentage of finer smaller than size *d* for the PSD-W and for the PSD-F of fraction *i*, respectively; andX_i is the initial mass percentage of fraction *i*. From Fig. 3, it can be observed that the PSD-Fs show more obvious changes than PSD-W in the polydisperse samples with the applied stress increasing from 0 to 6.4 MPa. This is possibly because the loss of coarse particles due to grain crushing can be compensated by the crushing of coarser particles. This implies that the amount of the breakage is always underestimated by using relative breakage indexes defined on the basis of the overall change of the PSD-W. In addition, it can be observed that the PSD-Fs, of uniform, gap-graded and polydisperse samples, all tend to be polydisperse and well- graded, similar to the evolution of the PSD-Ws of uniform samples. This strongly indicates that the evolution of the PSD-Fs also has a tendency to be self-similar. It is widely acknowledged that undergoing substantial grain crushing, the PSDs of granular materials becomes self-similar, also known as fractal. Herein based on the experimental results on the DGPs, the evolution of particle crushing can also be extended to the fractional particles in non-uniform samples.

Considering the surprising similarity in the evolution of fractional particle breakage in non-uniform samples, an interesting question arises as to whether the fractional particle breakage evolution paths for particles of the same size in different granular media are similar. And more generally, are the fractional particle

Table 1
Initial gradings, initial void ratios and applied vertical stresses of the DGP samples for 1D compression.

Sample ID	Fractional particle mass (g)						e_0	Vertical stress (MPa)
	15.9 mm	10.0 mm	6.3 mm	4.0 mm	2.5 mm	Total mass		
U1	600	–	–	–	–	600	1.506	0.8 ~ 6.4
U2	–	600	–	–	–	600	1.454	0.8 ~ 6.4
U3	–	–	600	–	–	600	1.405	0.8 ~ 6.4
U4	–	–	–	600	–	600	1.378	0.8 ~ 6.4
U5	–	–	–	–	600	600	1.371	0.8 ~ 6.4
M1	300	–	300	–	–	600	1.352	6.4
M2	–	300	300	–	–	600	1.401	0.8 ~ 6.4
M3	–	–	300	300	–	600	1.363	6.4
M4	–	–	300	–	300	600	1.232	6.4
M5	200	200	200	–	–	600	1.352	0.8 ~ 6.4
M6	150	150	150	150	–	600	1.266	0.8 ~ 6.4
M7	120	120	120	120	120	600	1.175	0.8 ~ 6.4

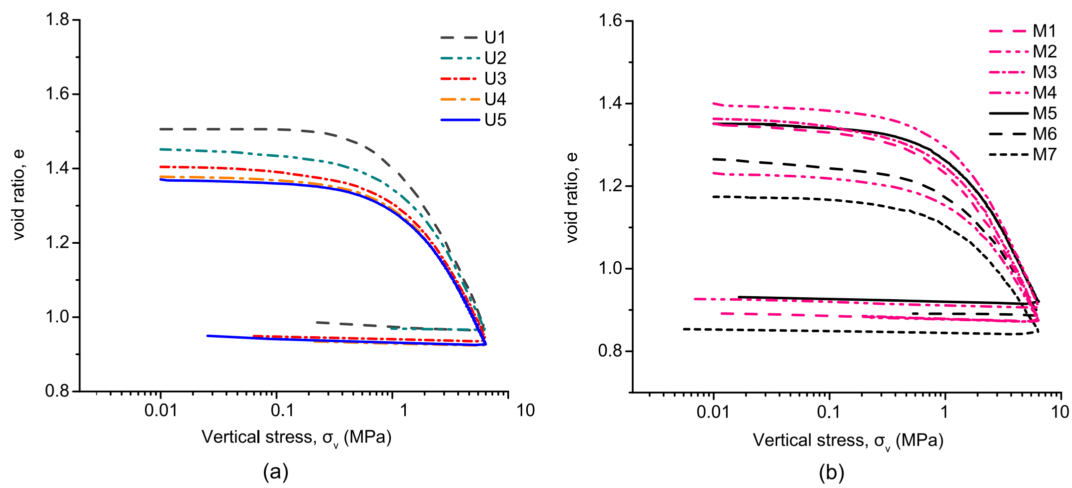

Fig. 2. $e - \log\sigma_v$ curves of DGP samples: (a) U1-U5; (b) M1-M7.

breakage evolution paths for particles of the same minerology but of different sizes in different granular samples similar?

To address the first question, the evolution of PSD-Fs of the particles with the same size in different samples are plotted on the same graph. The evolutions of the PSD-Ws of uniform samples are also plotted on the same graph. Fig. 4(a)~(e) are the evolutions of PSD-Fs for particles of 20.0–12.6, 12.6–7.9, 7.9–5.0, 5.0–3.1, and 3.1–2.0 mm, respectively. It can be observed that the curves are well stratified without obvious crossover in the figures. This result indicates that although the intensity of the fractional particle breakage depends on the PSD-W of the granular sample, the fractional breakage of the particles of the same size in different granular media do evolve along a unique path, which is also the same for the uniform particles. This means the breakage evolution path for particles of a given size is independent of the surrounding particles. The evolution paths for the PSD-Fs of particles of different sizes are not directly comparable. Nevertheless, if the particles are normalized by their initial characteristic particle sizes, we are able to experimentally address the second question. To this end, the particle sizes are normalized by their initial maximum sizes, and the normalized PSD-Fs of all the fractions of particles in polydisperse samples as well as in uniform samples from Fig. 4(a) to 4 (e) are put together in Fig. 4(f). These curves are surprisingly well-arranged, implying that the normalized breakage evolution paths of fractional particles are the same as those of the uniform particles, regardless of the particle size and the interaction of particles with different sizes. In contrast to the fractional particle breakage, the evolution of the PSD-Ws of different initial gradings intersect with each other, as shown in Fig. 5, implying that the particle breakage evolution paths for the whole samples are not unique.

The above experimental observations can be quantified by extending the definition of the relative breakage index in the breakage mechanics [34]. Einav assumed that the current PSD-W can be described by the linear interpolation of the initial and the fractal ultimate PSD-Ws, written as

$$P(d) = (1 - B_r)P_0(d) + B_r P_u(d) \tag{2}$$

where $P_0(d)$ is the initial PSD-W; $P_u(d)$ is the ultimate PSD-W; the coefficient B_r is defined as the relative breakage index ranging from 0 to 1. In this study, we extend this definition to describing the fractional particle breakage, written as

$$P_f(d_i,\ d) = (1 - B_r(d_i))P_{f0}(d_i,\ d) + B_r(d_i)P_{fu}(d_i,\ d) \tag{3}$$

where P_{f0}, P_f, and P_{fu} denote the initial, current and ultimate cumulative mass distribution for the fraction *i*. The assumption that the fractional PSD-Fs can be also represented by the linear interpolation of the initial and the ultimate PSD-Fs is proved tenable by conducting the linear regression analysis on the normalized PSDs in Fig. 4 (f). The ultimate fractal PSD-F is chosen to be $P_{f0}(d) = (d/d_M)^{0.7}$, where d_M is the maximum particle size in fraction *i*. The analysis results show that all PSD-Fs can be well fitted by the linear interpolation of the initial PSD-Fs and the ultimate fractal PSD-Fs, with the correlation coefficients greater than 0.98 for all the cases. In addition, the breakage indexes of each fractions are also calculated, as shown in Fig. 6.

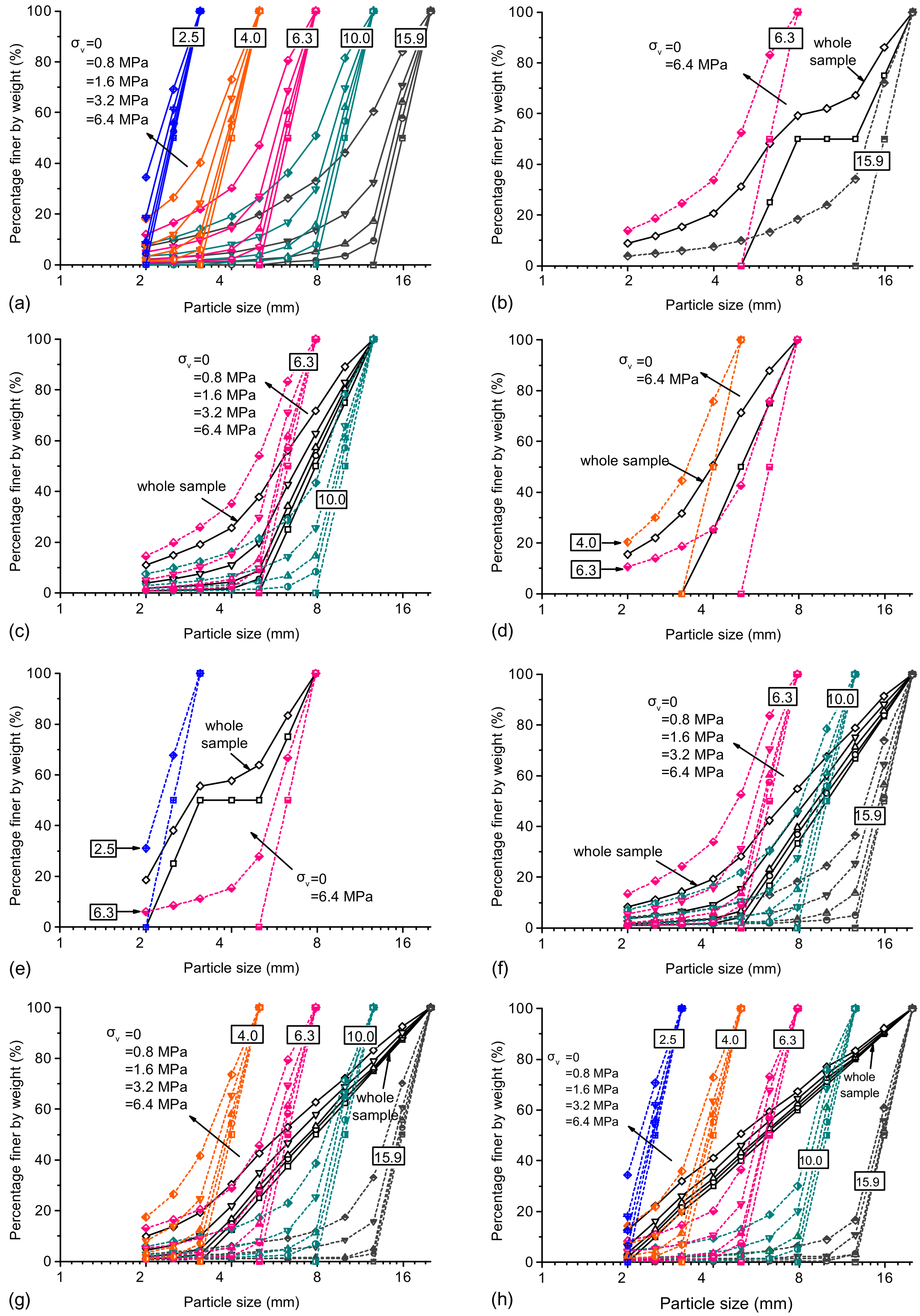

Fig. 3. PSD evolution curves of both the whole sample and of each fraction: (a) U1-U5; (b) M1; (c) M2; (d) M3; (e) M4; (f) M5; (g) M6; (h) M7.

For uniform samples, as shown in Fig. 6(a), the breakage indexes increase with increasing particle size because smaller particles have smaller volume and thus contain generally fewer defects [48]. For non-uniform particles, the breakage ratio of the largest particles is, on the contrary, the lowest among all particles. This interesting difference is because larger particles in a polydisperse granular medium is surrounded by smaller ones, which provides "hydrodynamic stress" in the large particles that protects the large particle from shearing failure [49–50]. Therefore, the fractional particle breakage of non-uniform particles is related to not only the crushing strength but also the contact number of surrounding particles. If the breakage indexes of different fractions

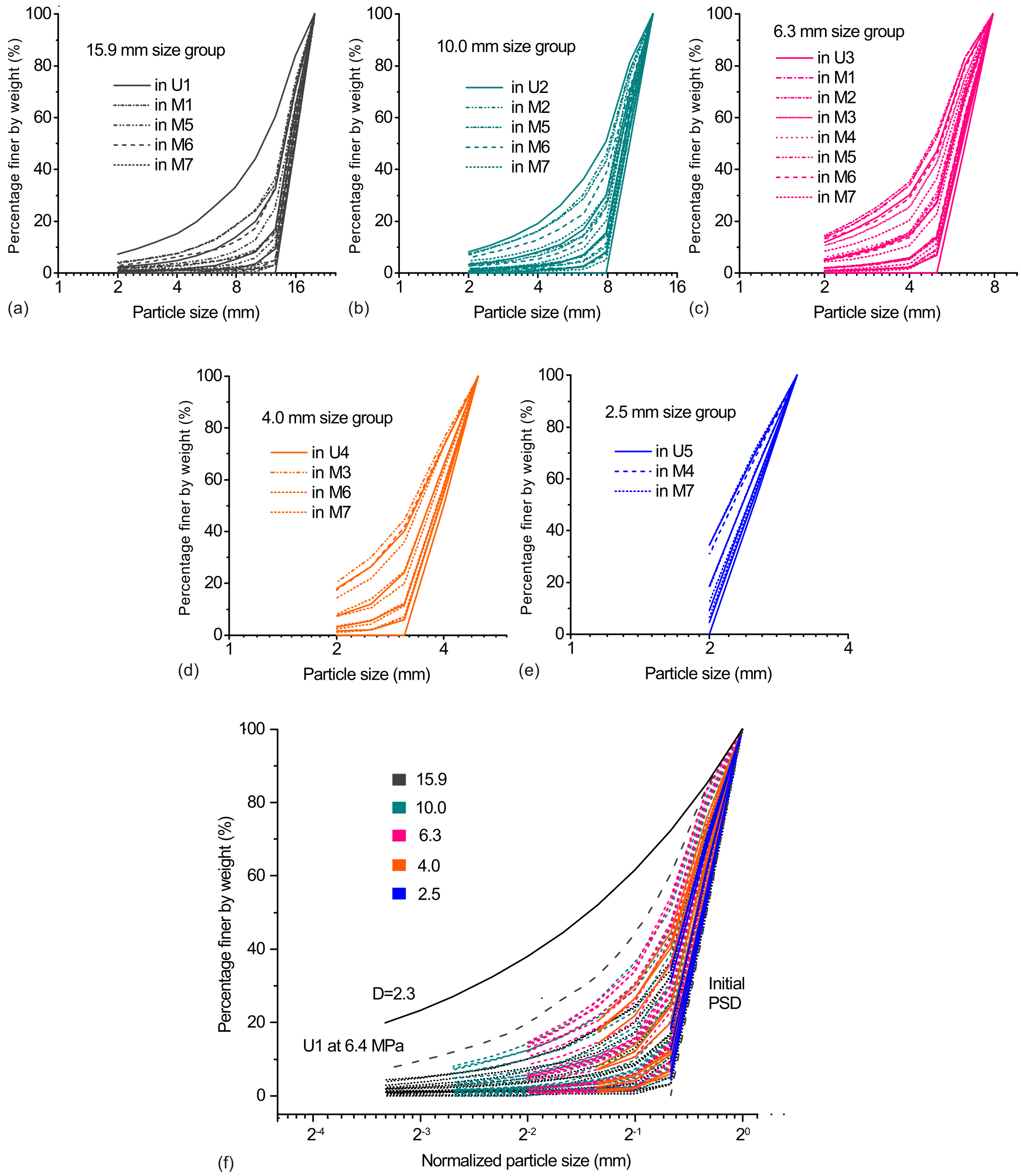

Fig. 4. The evolution paths of the PSD-Fs for: (a) 15.9 mm; (b)10.0 mm; (c) 6.3 mm; (d) 4.0 mm; (e) 2.5 mm; (f) all fractional particles on the normalized graph.

of particles in non-uniform samples can be predicted, the PSD of the whole sample can be calculated according to Eq (1) and (2). This will be further discussed in the next section.

3. Fractional particle breakage model

A complete particle breakage model should contain two key components: (1) a quantifiable index of the intensity and evolution path of the particle breakage, and (2) the relationship between what causes the particle breakage (e.g., magnitude of the stress, work input, etc.) and the quantifiable breakage index. Based on the results from the experiments on DGPs, it was found that the fractional breakage evolutions for particles of different sizes in a polydisperse granular medium follow the same path and the fractional breakage index $B_r(d)$ can be represented by the linear interpolation of the initial and ultimate PSD-Fs. Therefore, the major remaining question is how to establish the relationship between what causes the particle breakage and the quantifiable breakage index.

3.1. Definition of the fractional plastic work

A widely observed phenomenon in granular soils is that there is a unique relationship between the plastic work input per unit volume w_p^t and the amount of particle breakage, regardless of the loading path. This phenomenon was also theoretically supported by McDowell and Bolton [35] by assuming that the plastic work input is proportional to the creation of the new surface area during particle breakage. Thus, in this study, we choose the plastic work input as the triggering variable for the particle breakage. By definition, the plastic work input per unit volume for granular materials w_p^t is expressed as

$$w_p^t = \frac{W_p^t}{V_0^t} \tag{4}$$

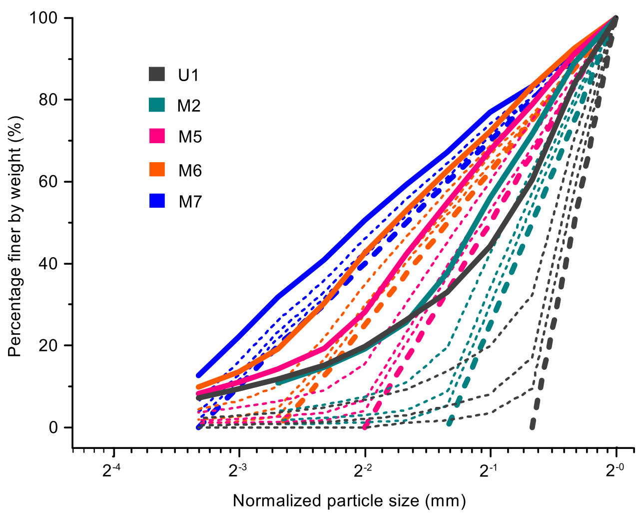

Fig. 5. The evolution paths for PSD-Ws for all the tested samples on the normalized graph: samples with unparallel initial gradings do not evolve along the same path.

where W_p^tdenotes the total plastic work input and V_0^t is the initial volume of the sample. For one-dimensional compression, the plastic work input can be calculated using the following expression

$$w_p^t = \int \sigma_v \mathrm{d}\varepsilon_v^p \tag{5}$$

where $\sigma_v$is the vertical stress and $\varepsilon_v^p$is the plastic volumetric strain. We plot the calculated $w_p^t$of samples U1-U5 using Eq. (5) against Einav's relative breakage index B_r in Fig. 7. It can be observed that B_r increases rapidly with w_p^tat the beginning of loading and the increasing trend slows down for higher plastic work input.

Eq. (4) is defined for whole granular specimens and is not able to depict the plastic work input into the particles within a certain size range in the polydisperse granular specimen. Herein with the reference of the definition of w_p^t, we define the fractional plastic work input per unit volume$w_p(d)$ as

$$w_p(d) = \frac{\mathrm{d}W_p(d)}{\mathrm{d}V_0(d)} \tag{6}$$

where $\mathrm{d}W_p(d)$denotes the plastic work input into the particles whose initial sizes range from d to d + dd; and $\mathrm{d}V_0(d)$is the initial volume of particles with sizes ranging from d to d + dd. For a granular material composed of homogenous particles, $\mathrm{d}V_0(d)$can be expressed as

$$\mathrm{d}V_0(d) = V_0^t p_0(d)\mathrm{d}d \tag{7}$$

where $p_0(d)$ denotes the initial volume/mass percentage of particles of size d.

It is worth remarking that from the microscopic point of view, it is difficult to allocate the frictional dissipations from the contact of two particles of different sizes. Thus, the concrete value of the frictional dissipation could depend on the arbitrarily-defined allocation law. In addition, it is also difficult to experimentally measure the fractional plastic work input. However, it should be guaranteed that the sum of the fractional plastic work input equals the total plastic work input measured in the representative volume element, given by

$$w_p^t = \int_{d_m}^{d_M} w_p(d)p_0(d)\mathrm{d}d \tag{8}$$

where d_m and d_M denote the minimum and maximum particle sizes, respectively.Here, without getting into the details of the allocation law, we assume that particles of size d to d + dd in a polydisperse granular medium require the same fractional plastic work input per unit volume as that in a uniform medium of composing of the same particles, as long as the fractional breakage indexes are equal. That is to say, the fractional $B_r(d) - w_p(d)$relationship for particles of a given size is assumed to be unique, independent of the size distribution of their surrounding particles. According to the experimental data of $B_r(d)$ shown in Fig. 6, we can estimate the fractional plastic work input per unit volume $w_p(d)$ for polydisperse samples through cubic spline interpolation of Fig. 7. The estimated $w_p(d)$ is plotted in Fig. 8. It is seen that small particles require more energy input in a polydisperse sample. It is also possible to numerically calculate the total plastic work using the

discretized form of Eq. (9), written as

$$w_{p\_calcul}^t = \sum_{i=1}^{N} X_i w_p(d_i) \tag{9}$$

where$d_i$denotes the characteristic particle size of size range i (i = 1, 2, 3, ..., N); and X_i denotes the mass fraction (or volume fraction for homogenous particles) of particles of initial characteristic size d_i. Fig. 8 plots the experimentally measured total plastic work input together with the numerically calculated total plastic work using Eq. (9) of M2, M5, M6 and M7. The data of M1, M3 and M4 are not shown because only one vertical stress was applied for these three specimens. It is seen that the estimated total plastic work agrees basically with the experimentally measures ones, indicating that the defined fractional plastic work is acceptable and that the $B_r(d) - w_p(d)$relationship for particles of a given size is indeed unique.

3.2. Distribution of the fractional plastic work

The plastic work into a polydisperse granular system is not uniformly distributed as a function of the particle size. It is readily seen in Fig. 8 that smaller particles tend to require more plastic work to reach the same amount of particle breakage than bigger particles. Before quantifying the distribution of the plastic work in the system, the plastic work input should be normalized, given as

$$\theta(d) = \frac{w_p(d)p_0(d)}{w_p^t} \tag{10}$$

where $\theta(d)$is defined as the probability density of the plastic work in the system. Thus, $\theta(d)\mathrm{d}d$denotes the probability of the plastic work into particles of size from d to d + dd.

Combining Eqs. (6), (8) and (10), we can obtain the normalizing condition

$$\int_{d_m}^{d_M} \theta(d)\mathrm{d}d = 1 \tag{11}$$

Fig. 9 plots the normalized fractional plastic work against the particle size for different polydisperse samples at different stress levels on $\ln\theta(d) - d$ axes. It is seen from the figure that the $\ln\theta(d) - d$ data can be fitted by straight lines, regardless of the applied stress, given by

$$\ln\theta(d) = \beta d + C \tag{12}$$

where βdenotes the slope of the fitting line and C denotes the $\ln\theta(d)$-intercept. It can be also observed in Fig. 9 that the $\theta(d) - d$ relationship for a given granular sample does not change appreciably with the applied stress. Thus, both $\beta$and C can be regarded as constants for a given granular material.

Combining Eqs. (11) and (12) yields

$$\theta(d) = \frac{\beta e^{\beta d}}{e^{\beta d_M} - e^{\beta d_m}} \tag{13}$$

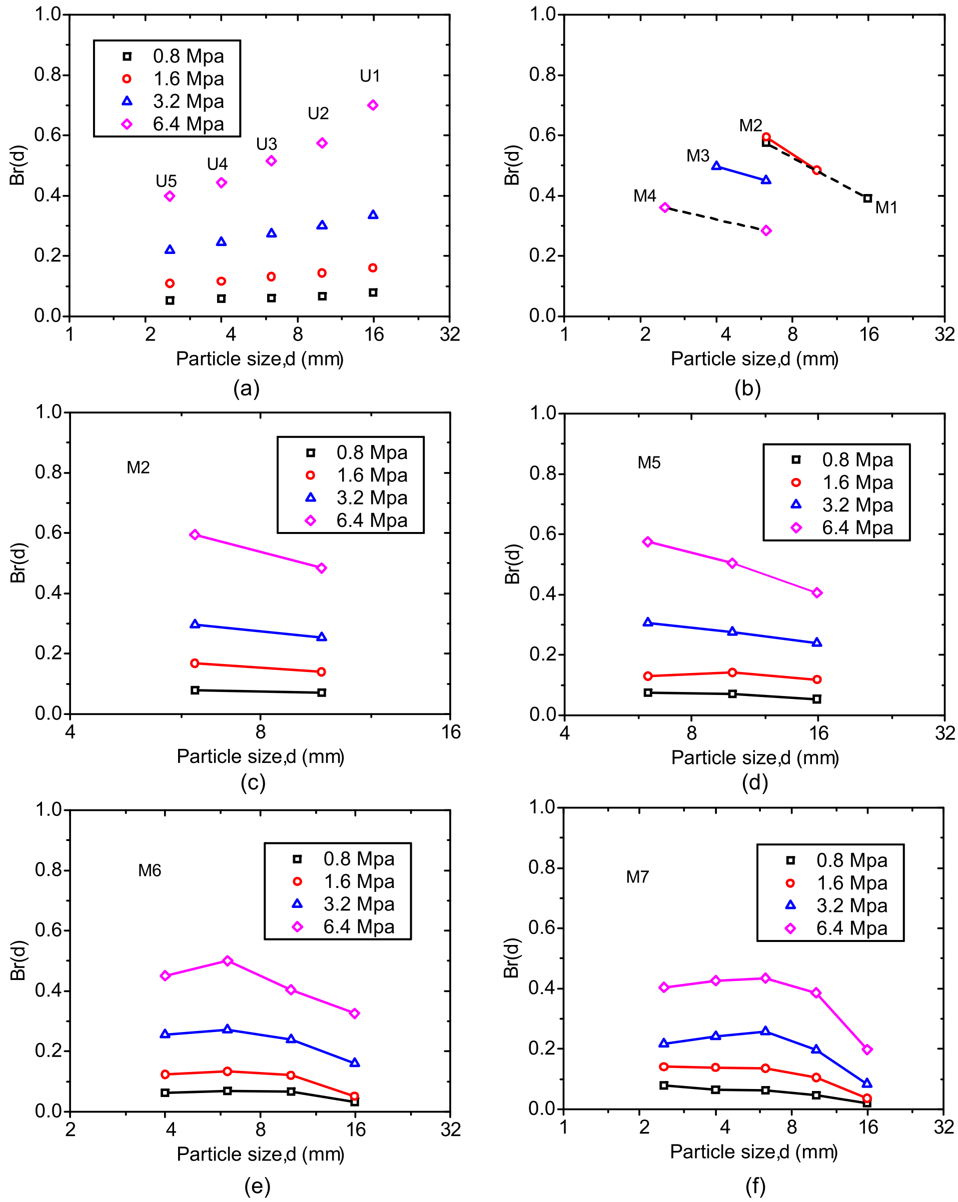

Fig. 6. Distributions of the fractional breakage index in different samples: (a) U1-U5; (b) M1-M4 at 6.4 MPa; (c) M2; (d) M5; (e) M6; (f) M7.

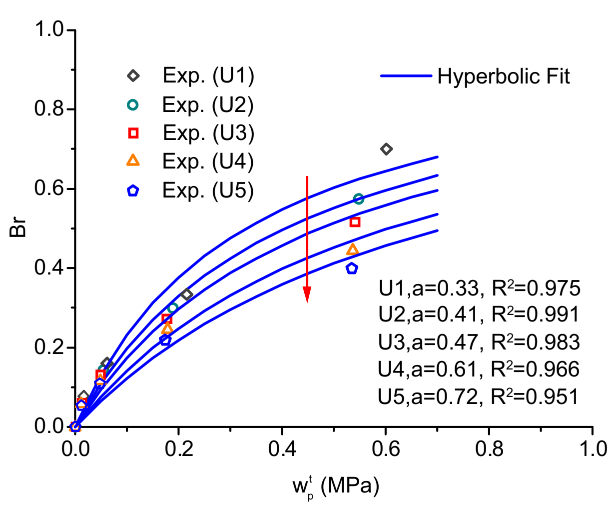

Fig. 7. The breakage indexes against the plastic work for uniform samples.

It is noted that the distribution of $\theta(d)$ does not depend on the parameter C. The parameter β is related to the initial PSD of the material.

Substituting Eq. (13) into Eq. (10), we can obtain

$$w_p(d) = \frac{w_p^t \beta e^{\beta d}}{e^{\beta d_M} - e^{\beta d_m}} / p_0(d) \tag{14}$$

3.3. Fractional breakage-plastic work relationship considering size effect

The $B_r - w_p^t$ relationship is often described by a hyperbolic function [33,51–53], given by

$$B_r = \frac{w_p^t}{a + w_p^t} \tag{15}$$

where a is constant for a given granular material. It is seen in Fig. 7 that the fitting curves using Eq. (15) agree basically with the experimental data.

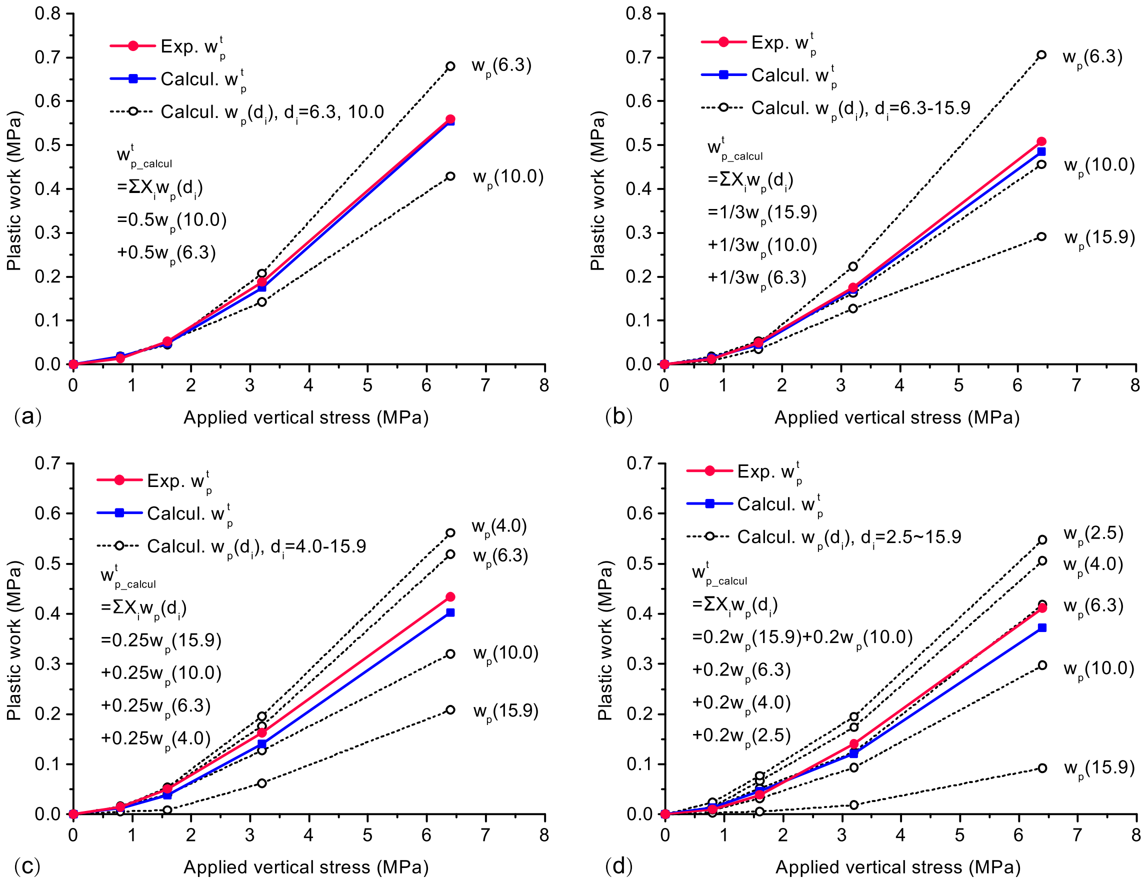

Fig. 8. Comparison of the calculated w_p^t and the experimental results: (a) M2; (b) M5; (c) M6; (d) M7.

The differential form of Eq. (15) leads to

$$\mathrm{d}B_r = \frac{a}{\left(a + w_p^t\right)^2}\mathrm{d}w_p^t \tag{16}$$

At the initial loading state, we have $w_p = 0$ and Eq. (16) is degenerated into

$$\mathrm{d}w_p^t = a\mathrm{d}B_r \tag{17}$$

Eq. (17) indicates that the parameter a denotes the plastic work per unit increase of the breakage index at the initial loading state.

Eq. (17) can be also extended to the fractional particle breakage, written as

$$B_r(d) = \frac{w_p(d)}{a + w_p(d)} \tag{18}$$

Although the $B_r(d) - w_p(d)$ relationship in a polydisperse granular media is independent of the PSD of the surrounding particles, the experimental results shown in Fig. 8 indicate that it depends on the particle size d. It is widely accepted that the probability for a brittle block of characteristic size d to survive a tensile stress σobeys the Weibull distribution [48], given by

$$P_s(\sigma, d) = \exp\left[-\left(\frac{d}{d_0}\right)^3\left(\frac{\sigma}{\sigma_0}\right)^m\right] \tag{19}$$

where P_s is the survival probability of the particle; d_0 and$\sigma_0$are the reference particle size and the reference stress, respectively; m is the Weibull modulus, which is a material constant. Eq. (19) has been experimentally verified for single sand particles under plate loading and within triaxial loading conditions for different granular particles [44]. It was demonstrated by McDowell and Bolton [35] that if the failure of a particle is defined statistically by the survival probability lower than a threshold, the size effect of the crushing strength of a particle can be obtained from Eq. (19):

$$\text{If } P_s(\sigma, d) = const., \text{ then } \sigma \propto d^{-3/m} \tag{20}$$

Several researchers [9,52] further proved that Eq. (20) can be also extended to granular assemblies.

Consider two geometrically similar granular samples I and II, with different characteristic particle sizes d_1 and d_2. Their breakage yield stress should satisfy

$$\frac{\sigma_1}{\sigma_2} = \left(\frac{d_1}{d_2}\right)^{-\lambda} \tag{21}$$

where $\lambda = 3/m$. Frossard et al. [51] argued further that when the physical similarity is achievable for both samples, the geometric similarity means the irreversible deformations of both samples are equal. Thus, the plastic work for both samples at the initial loading can be linked via

$$\frac{w_p(d_1)}{w_p(d_2)} = \frac{\sigma_1}{\sigma_2} = \left(\frac{d_1}{d_2}\right)^{-\lambda} \tag{22}$$

It should be remarked that Eq. (22) is only valid for the initial loading (with small value ofB_r) because the similarity of the PSDs between the two granular assemblies cannot be guaranteed when substantial grain crushing occurs.

For the samples I and II, comparing Eqs. (18) and (22), we can obtain the scale effect of the parameter a

$$\frac{a_1}{a_2} = \left(\frac{d_1}{d_2}\right)^{-\lambda} \tag{23}$$

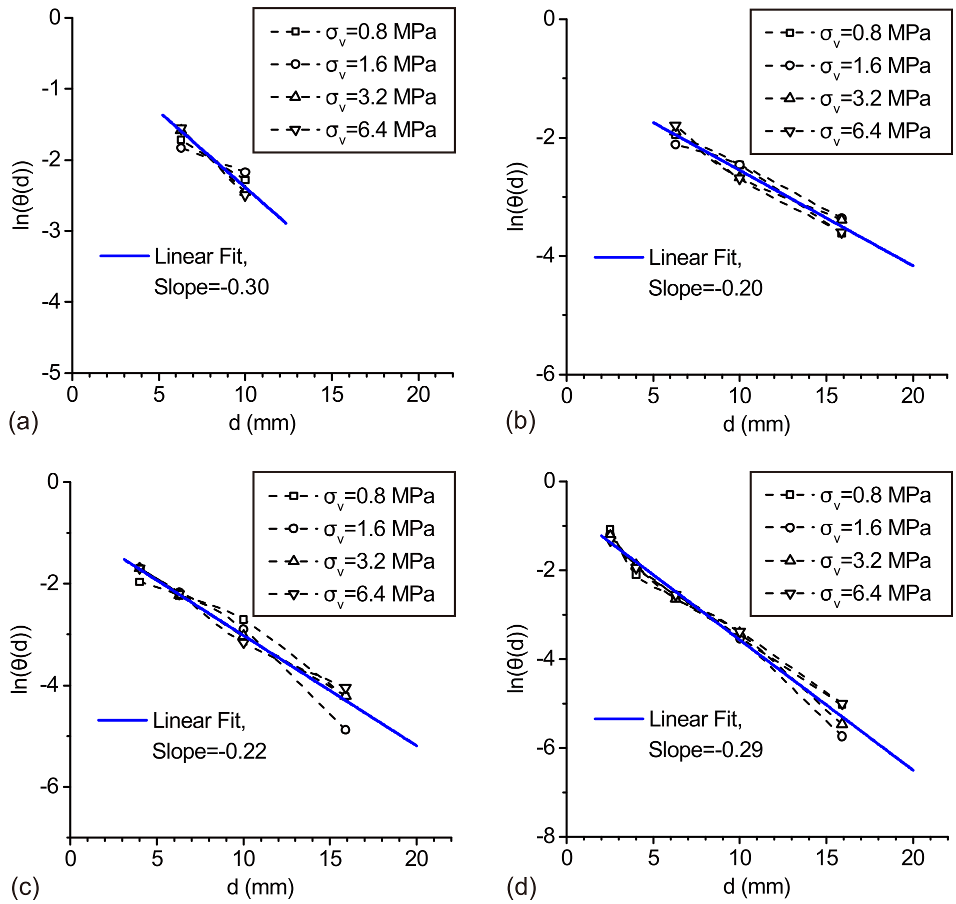

Fig. 9. Linear fitting of $\ln(\theta(d))$ against size: (a) M2; (b) M5; (c) M6; (d) M7.

Experimental results of samples U1-U5, as given in Fig. 10, also show that the relationship between parameter a and the particle size d can be represented by a straight line in double logarithmic axes, agreeing with Eq. (23). Therefore, for the sake of simplicity, we define

$$a = \alpha d^{-\lambda} \tag{24}$$

where $\alpha$is a size-independent material parameter.

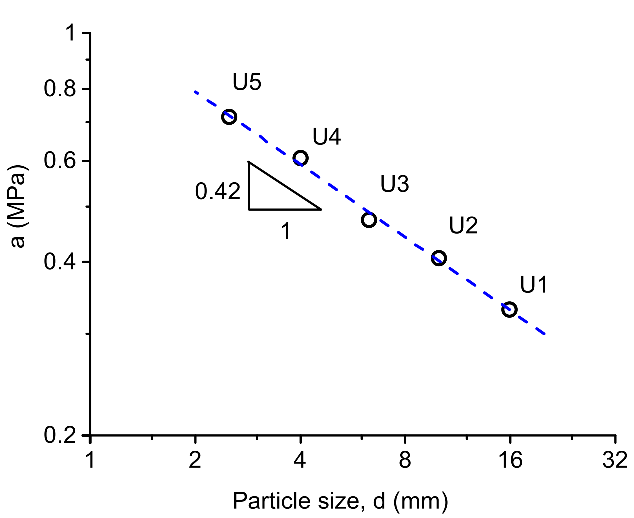

Fig. 10. Size-dependence of the parameter a plotted on the double logarithmic axes.

Substituting Eq. (24) into Eq. (18), one has the relationship between the plastic work and the breakage index accounting for the size effect, given by

$$B_r(d) = \frac{w_p(d)}{\alpha d^{-\lambda} + w_p(d)} \tag{25}$$

Fig. 11 compares the experimentally $B_r(d) - w_p(d) - d$ relationships of granular samples U1-U5 with the predicted results by Eq. (25). In Eq. (25), the values of the parameters are fitted to be $\alpha = 1.06$,$\lambda = 0.42$, respectively. It is seen in Fig. 11 that the model prediction agrees well with the experimental results, indicating that Eq. (25) is capable of describing the $B_r(d) - w_p(d)$ relationships of granular soils with different characteristic sizes using only one set of parameters.

3.4. Complete fractional particle breakage model and model performance

Combining the distribution of the fractional plastic work (given in Eq. (14)) and the fractional breakage-plastic work relationship considering size effect (given in Eq. (25)) leads to the fractional particle breakage model

$$B_r(d) = \frac{\frac{w_p^t \beta e^{\beta d}}{e^{\beta d_M} - e^{\beta d_m}} / p_0(d)}{\alpha d^{-\lambda} + \frac{w_p^t \beta e^{\beta d}}{e^{\beta d_M} - e^{\beta d_m}} / p_0(d)} \tag{26}$$

Fig. 12 compares the experimentally obtained fractional particle breakage of samples M2, M3, M6 and M7 with the calculated results using Eq. (26) at different loading stages. It is seen that

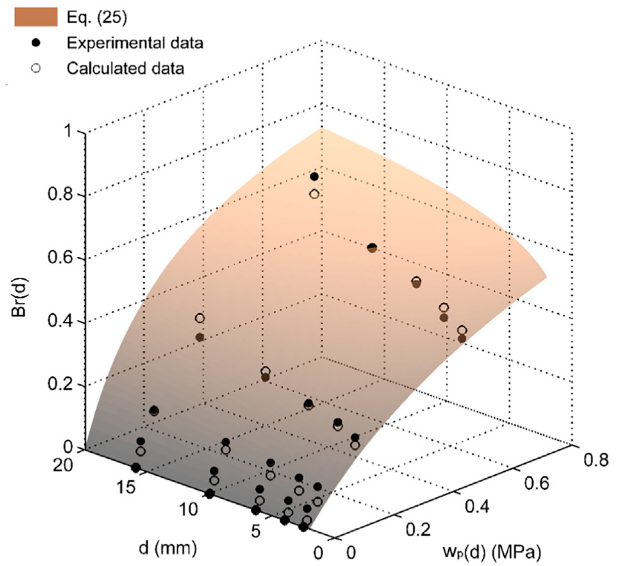

Fig. 11. Comparison of the calculated $B_r(d)$ with the experimental results in $B_r(d) - w_p(d) - d$ space.

the calculated fractional particle breakage shows good agreement with the experimental data. Moreover, Fig. 12 indicates that Eq. (26) is not only able to describe the monotonically decreasing trend for the fractional breakage index with the particle size (see sample M2), but also the first increasing and then decreasing trend for the fractional particle breakage index with the particle size (see samples M5, M6 and M7).

The evolution of the fractional PSDs can be calculated by the linear interpolation of the initial and the fractal fractional PSDs. The evolution of the overall cumulative PSD can then be calculated by the integration of the weighted fractional PSD, written as

$$P(d) = \int_{d_m}^{d_M} p_0(\Delta)P_f(\Delta,\ d)\mathrm{d}\Delta \tag{27}$$

where $p_0(\Delta)\mathrm{d}\Delta$ denotes the initial probability (before particle breakage) of a particle to exist within the size range $\Delta$to $\Delta + \mathrm{d}\Delta$; and $P_f(\Delta,\ d)$ denotes the cumulative PSD of the particles with initial sizes ranging from $\Delta$to $\Delta + d\Delta$, calculated by

$$P_f(\Delta, d) = (1 - B_r(\Delta))P_{f0}(\Delta, d) + B_r(\Delta)P_{fu}(\Delta, d) \tag{28}$$

Combing Eqs. (26), (27) and (28), we can predict the breakage evolution of a polydisperse sample by knowing the total plastic work. Fig. 13 gives two examples of the calculated evolution of the overall PSDs using the fractional particle breakage model.

The first example is the evolution of the PSD of the sample M6. The parameters in the proposed fractional breakage model are listed in Fig. 13 (a), which were calibrated in the previous sections. It is seen that the model prediction agrees well with the experimentally-measured PSDs at different applied stress levels. We also added the test of sample M6 at 12.8 MPa, it is seen that the predicted results still agree well with the experimental results.

The second example is the large triaxial test results on rockfill materials by Marachi et al. [54]. The reason that we choose this test results is because of the following reasons: 1) the initial PSD of the tested material is highly polydisperse and the initial grading curve partially surpassed the theoretical fractal distribution, resulting in the difficulty in using Einav's breakage index to describe the evolu-

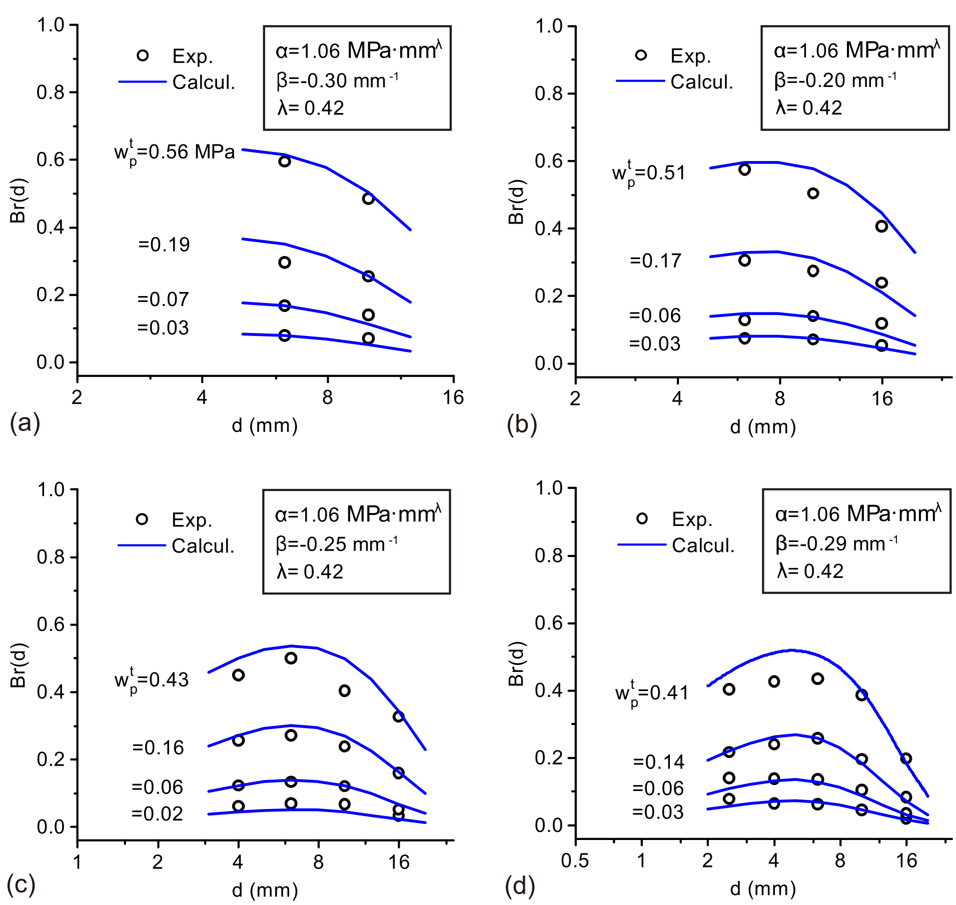

Fig. 12. Comparison of the calculated $B_r(d)$ with the experimental results: (a) M2; (b) M5; (c) M6; (d) M7.

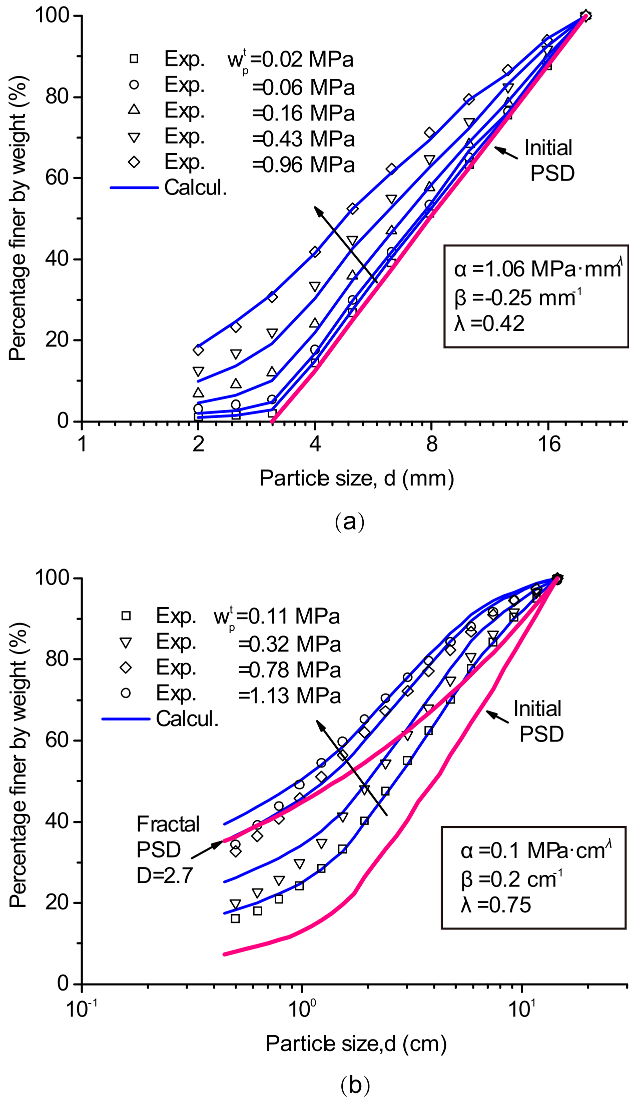

Fig. 13. Comparison of the predicted PSD evolution with the experimental results for: (a) M6; (b) Marachi et al. (1969).

tion of the PSD. 2) The rockfill material was loaded in triaxial condition, providing a good opportunity to verify whether the proposed model is able to describe the particle breakage in shearing loading. The ultimate fractal PSD of each fraction of particles is chosen to be $P_u(d) = (d/d_M)^{0.3}$, with the fractal dimension equaling 2.5. The plastic work input of triaxial tests is calculated by the following expression

$$w_p^t = \int \sigma_1 d\varepsilon_1^p + 2\int \sigma_3 d\varepsilon_3^p \tag{29}$$

where $\sigma_1$and $\sigma_3$denotes the major and minor principle stresses, respectively; $d\varepsilon_1^p$ and $d\varepsilon_3^p$are the plastic major and minor principle strain increments, respectively(see reference [50,54]). The plastic work at different confining stresses were calculated to be 0.11, 0.32, 0.78, 1.13 MPa, respectively. Fig. 12(b) shows that the calculated evolution of the PSD agrees very well with the experimental results, suggesting that the proposed fractional particle breakage model is suitable for describing the evolution of the PSD of granular materials under different loading conditions, in spite of the simplicity of the model.

4. Conclusions

This paper aims to establish a unified fractional particle breakage model for granular materials. For this purpose, a novel experimental method, which consists of using DGPs to track the fractional particle breakage in granular assemblies was first adopted. The fractional particle breakage model, was then proposed based on the experimental observations. The following conclusions can be drawn from this study: the fractional particle breakage evolutions for particles of different sizes in a polydisperse granular medium, or in different uniformly distributed granular assemblies, all follow the same path, which can be further represented by the linear interpolation of the initial and the ultimate fractal PSDs.

Based on the hypothesis of a unique particle breakage evolution path, a unified fractional particle breakage model was further proposed. The proposed model contains two key features: 1) the fractional plastic work was defined and the distribution of the normalized fractional plastic work in a polydisperse granular assembly satisfies a unique exponential distribution, regardless of the evolution of the PSDs. 2) The widely used hyperbolic breakage-plastic work relationship was extended for the fractional particle breakage by considering the size effect of particle breakage. The evolution of the overall PSD during particle breakage can be obtained by summing the fractional PSDs. The proposed model contains 3 parameters α,λ and β, related to the strength of the particles, the size effect of the particle strength and the effect of the initial PSD of the assembly, respectively.

Although the proposed model is based on the one-dimensional compression tests on crushable DGPs, the performance of the model in other stress paths is also verified by the experimental results of a rockfill material under triaxial loading in the literature. The proposed model differs from other particle breakage models defined in the continuum mechanics contexts in that it is able to capture better the evolution of the overall PSD of granular materials, even when the initial PSD of the granular material surpass partially the theoretical fractal PSD. Hence, the proposed model provides a useful tool for the understanding and prediction of detailed and precise particle breakage of granular materials with polydisperse PSDs.

CRediT authorship contribution statement

Chao-Min Shen: Conceptualization, Methodology, Writing - original draft. **Ji-Du Yu:** Investigation, Formal analysis, Writing - original draft. **Si-Hong Liu:** Project administration, Writing - review & editing. **Hang-Yu Mao:** Investigation, Software.

Declaration of Competing Interest

The authors declare that they have no known competing financial interests or personal relationships that could have appeared to influence the work reported in this paper.

Acknowledgements

The financial supports of the National Natural Science Foundation of China (Grant Nos. U1765205; 51979091, 52009036) and the Postgraduate Research & Practice Innovation Program of Jiangsu Province (Grant No. KYCX20_0544) are greatly acknowledged.

References

[1] Y. Guo, V. Markine, J. Song, G. Jing, Ballast degradation: Effect of particle size and shape using Los Angeles Abrasion test and image analysis, Constr. Build. Mater. 169 (2018) 414–424.

[2] W. Mao, S. Aoyama, I. Towhata, A study on particle breakage behavior during pile penetration process using acoustic emission source location, Geosci. Front. (2019).
[3] E. Ganju, F. Han, M. Prezzi, R. Salgado, J.S. Pereira, Quantification of displacement and particle crushing around a penetrometer tip, Geosci. Front. (2020).
[4] C. Li, J. Zheng, Z. Zhang, A. Sha, J. Li, Morphology-based indices and recommended sampling sizes for using image-based methods to quantify degradations of compacted aggregate materials, Constr. Build. Mater. 230 (2020) 116970.
[5] V. Nardelli, M.R. Coop, J.E. Andrade, F. Paccagnella, An experimental investigation of the micromechanics of Eglin sand, Powder Technol. 312 (2017) 166–174.
[6] L. Liu, G. Cai, S. Liu, Compression properties and micro-mechanisms of rubber-sand particle mixtures considering grain breakage, Constr. Build. Mater. 187 (2018) 1061–1072.
[7] G. Ma, R.A. Regueiro, W. Zhou, Q. Wang, J. Liu, Role of particle crushing on particle kinematics and shear banding in granular materials, Acta Geotech. 13 (3) (2018) 601–618.
[8] C.M. Shen, S.H. Liu, Y.S. Wang, Microscopic interpretation of one-dimensional compressibility of granular materials, Comput. Geotech. 91 (2017) 161–168.
[9] C.M. Shen, S.H. Liu, L.J. Wang, Y.S. Wang, Micromechanical modeling of particle breakage of granular materials in the framework of thermomechanics, Acta Geotech. 14 (4) (2019) 939–954.
[10] D.M. Wood, K. Maeda, Changing grading of soil: effect on critical state, Acta Geotech. 3 (1) (2008) 3–14.
[11] F.N. Altuhafi, M.R. Coop, Changes to particle characteristics associated with the compression of sands, Géotechnique 61 (6) (2011) 459–471.
[12] W.M. Yan, Y. Shi, Evolution of grain grading and characteristics in repeatedly reconstituted assemblages subject to one-dimensional compression, Geotech. Lett. 4 (3) (2014) 223–229.
[13] Y. Jia, B. Xu, S. Chi, B. Xiang, Y. Zhou, Research on the particle breakage of rockfill materials during triaxial tests, Int. J. Geomech. 17 (10) (2017) 04017085.
[14] J. Zhang, M. Li, Z. Liu, N. Zhou, Fractal characteristics of crushed particles of coal gangue under compaction, Powder Technol. 305 (2017) 12–18.
[15] Y. Xu, The fractal evolution of particle fragmentation under different fracture energy, Powder Technol. 323 (2018) 337–345.
[16] Y. Xiao, Z. Yuan, Y. Lv, L. Wang, H. Liu, Fractal crushing of carbonate and quartz sands along the specimen height under impact loading, Constr. Build. Mater. 182 (2018) 188–199.
[17] B. Zhao, J. Wang, M.R. Coop, G. Viggiani, M. Jiang, An investigation of single sand particle fracture using X-ray micro-tomography, Géotechnique 65 (8) (2015) 625–641.
[18] R.C. Hurley, S.A. Hall, J.E. Andrade, J. Wright, Quantifying interparticle forces and heterogeneity in 3D granular materials, Phys. Rev. Lett. 117 (9) (2016) 098005.
[19] Z. Li, L. Liu, S. Yan, M. Zhang, Y. Xie, Properties of microscopic particle morphology and particle contact of renewable construction waste mixtures, Constr. Build. Mater. 207 (2019) 190–205.
[20] W. Wang, M.R. Coop, An investigation of breakage behaviour of single sand particles using a high-speed microscope camera, Géotechnique 66 (12) (2016) 984–998.
[21] M.C. Todisco, W. Wang, M.R. Coop, K. Senetakis, Multiple contact compression tests on sand particles, Soils and Found. 57 (1) (2017) 126–140.
[22] D.M. Kusumawardani, Y.D. Wong, The influence of aggregate shape properties on aggregate packing in porous asphalt mixture (PAM), Constr. Build. Mater. 255 (2020) 119379.
[23] J. Eliáš, Simulation of railway ballast using crushable polyhedral particles, Powder Technol. 264 (2014) 458–465.
[24] T. Afshar, M.M. Disfani, A. Arulrajah, G.A. Narsilio, S. Emam, Impact of particle shape on breakage of recycled construction and demolition aggregates, Powder Technol. 308 (2017) 1–12.
[25] J. Zhang, J. Li, Y. Yao, J. Zheng, F, Gu, Geometric anisotropy modeling and shear behavior evaluation of graded crushed rocks, Constr. Build. Mater. 183 (2018) 346–355.
[26] G.R. McDowell, J.P. de Bono, On the micro mechanics of one-dimensional normal compression, Géotechnique 63 (11) (2013) 895–908.
[27] M.O. Ciantia, M. Arroyo, F. Calvetti, A. Gens, An approach to enhance efficiency of DEM modelling of soils with crushable grains, Géotechnique 65 (2) (2015) 91–110.
[28] A.B. Kh, A.A. Mirghasemi, S. Mohammadi, Numerical simulation of particle breakage of angular particles using combined DEM and FEM, Powder Technol. 205 (1–3) (2011) 15–29.
[29] G. Ma, W. Zhou, X.L. Chang, M.X. Chen, A hybrid approach for modeling of breakable granular materials using combined finite-discrete element method, Granul. Matter 18 (1) (2016) 7.
[30] G. Ma, W. Zhou, X.L. Chang, Modeling the particle breakage of rockfill materials with the cohesive crack model, Comput. Geotech. 61 (2014) 132–143.
[31] F. Zhu, J. Zhao, A peridynamic investigation on crushing of sand particles, Géotechnique 69 (6) (2019) 526–540.
[32] B.O. Hardin, Crushing of soil particles, J. Geotechn. Eng. 111 (10) (1985) 1177–1192.
[33] P.V. Lade, J.A. Yamamuro, P.A. Bopp, Significance of particle crushing in granular materials, J. Geotech. Eng. 122 (4) (1996) 309–316.
[34] I. Einav, Breakage mechanics-part I, theory, J. Mech. Phys. Solids 55 (6) (2007) 1274–1297.
[35] G.R. McDowell, M.D. Bolton, D. Robertson, The fractal crushing of granular materials, J. Mech. Phys. Solids 44 (12) (1996) 2079–2102.
[36] Y. Nakata, F.L. Hyde, M. Hyodo, H. Murata, A probabilistic approach to sand particle crushing in the triaxial test, Géotechnique 49 (5) (1999) 567–583.
[37] J. Huang, S. Xu, H. Yi, S. Hu, Size effect on the compression breakage strengths of glass particles, Powder Technol. 268 (2014) 86–94.
[38] B. Zhou, J. Wang, H. Wang, A new probabilistic approach for predicting particle crushing in one-dimensional compression of granular soil, Soils Found. 54 (4) (2014) 833–844.
[39] Y. Li, S. Zhang, R. Wang, Y. Zhao, C. Men, Effects of carbonation treatment on the crushing characteristics of recycled coarse aggregates, Constr. Build. Mater. 201 (2019) 408–420.
[40] N.H. Minh, Y.P. Cheng, A DEM investigation of the effect of particle-sized distribution on one-dimensional compression, Géotechnique 63 (1) (2013) 44–53.
[41] G.R. McDowell, M.D. Bolton, On the micromechanics of crushable aggregates, Géotechnique 48 (5) (1998) 667–679.
[42] S. Zhang, C.X. Tong, X.D. Li, Sheng, A new method for studying the evolution of particle breakage, Géotechnique 65 (11) (2015) 911–922.
[43] C.X. Tong, K.F. Zhang, S. Zhang, D. Sheng, A stochastic particle breakage model for granular soils subjected to one-dimensional compression with emphasis on the evolution of coordination number, Comput. Geotech. 112 (2019) 72–80.
[44] Y. Nakata, M.A. Hyodo, F.L. Hyde, Y. Kato, H. Murata, Microscopic particle crushing of sand subjected to high pressure one-dimensional compression, Soils Found. 41 (1) (2001) 69–82.
[45] W.X. Xu, Y. Jiao, Theoretical framework for percolation threshold, tortuosity and transport properties of porous materials containing 3D non-spherical pores, Int. J. Eng. Sci. 134 (2019) 31–46.
[46] Z. Zhu, W. Xu, H. Chen, The fraction of overlapping interphase around 2D and 3D polydisperse non-spherical particles: Theoretical and numerical models, Comput. Method Appl. M. 345 (2019) 728–747.
[47] J.D. Yu, C.M. Shen, S.H. Liu, Y.P. Cheng, Exploration of the survival probability and shape evolution of crushable particles during one-dimensional compression using dyed gypsum particles, J. Geotech. Geoenviron. (2020), https://doi.org/10.1061/(ASCE)GT.1943-5606.0002371.
[48] W. Weibull, Stockholm, and Sweden. A statistical distribution function of wide applicability, J. Appl. Mech. 13 (1951) 293–297.
[49] C. Sammis, G. King, R. Biegel, The kinematics of gouge deformation, Pure Appl. Geophys. 125 (5) (1987) 777–812.
[50] O. Tsoungui, D. Vallet, J.C. Charmet, Numerical model of crushing of grains inside two-dimensional granular materials, Powder Technol. 105 (1–3) (1999) 190–198.
[51] Z.Y. Yin, P.Y. Hicher, C. Dano, Y.F. Jin, Modeling mechanical behavior of very coarse granular materials, J. Eng. Mech. 143 (1) (2017) C4016006.
[52] E. Frossard, W. Hu, C. Dano, P.Y. Hicher, Rockfill shear strength evaluation: a rational method based on size effects, Géotechnique 62 (5) (2012) 415–427.
[53] B.Y. Zhang, Y.X. Jie, D.Z. Kong, Particle size distribution and relative breakage for a cement ellipsoid aggregate, Comput. Geotech. 53 (2013) 31–39.
[54] N. Marachi, C. Chan, H. Seed, J. Duncan, Strength and Deformation Characteristics of Rockfill Materials, University of California, Berkeley, CA, 1969.